ARTICLES

Folding DNA to create nanoscale shapes and patterns

Paul W. K. Rothemund[1]

'Bottom-up fabrication', which exploits the intrinsic properties of atoms and molecules to direct their self-organization, is widely used to make relatively simple nanostructures. A key goal for this approach is to create nanostructures of high complexity, matching that routinely achieved by 'top-down' methods. The self-assembly of DNA molecules provides an attractive route towards this goal. Here I describe a simple method for folding long, single-stranded DNA molecules into arbitrary two-dimensional shapes. The design for a desired shape is made by raster-filling the shape with a 7-kilobase single-stranded scaffold and by choosing over 200 short oligonucleotide 'staple strands' to hold the scaffold in place. Once synthesized and mixed, the staple and scaffold strands self-assemble in a single step. The resulting DNA structures are roughly 100 nm in diameter and approximate desired shapes such as squares, disks and five-pointed stars with a spatial resolution of 6 nm. Because each oligonucleotide can serve as a 6-nm pixel, the structures can be programmed to bear complex patterns such as words and images on their surfaces. Finally, individual DNA structures can be programmed to form larger assemblies, including extended periodic lattices and a hexamer of triangles (which constitutes a 30-megadalton molecular complex).

In 1959, Richard Feynman put forward the challenge of writing the *Encyclopaedia Britannica* on the head of a pin[1], a task which he calculated would require the use of dots 8 nm in size. Scanning probe techniques have essentially answered this challenge: atomic force microscopy[2] (AFM) and scanning tunnelling microscopy[3,4] (STM) allow us to manipulate individual atoms. But these techniques create patterns serially (one line or one pixel at a time) and tend to require ultrahigh vacuum or cryogenic temperatures. As a result, methods based on self-assembly are considered as promising alternatives that offer inexpensive, parallel synthesis of nanostructures under mild conditions[5]. Indeed, the power of these methods has been demonstrated in systems based on components ranging from porphyrins[6] to whole viral particles[7]. However, the ability of such systems to yield structures of high complexity remains to be demonstrated. In particular, the difficulty of engineering diverse yet specific binding interactions means that most self-assembled structures contain just a few unique positions that may be addressed as 'pixels'.

Nucleic acids can help overcome this problem: the exquisite specificity of Watson–Crick base pairing allows a combinatorially large set of nucleotide sequences to be used when designing binding interactions. The field of 'DNA nanotechnology'[8,9] has exploited this property to create a number of more complex nanostructures, including two-dimensional arrays with 8–16 unique positions and less than 20 nm spacing[10,11], as well as three-dimensional shapes such as a cube[12] and truncated octahedron[13]. However, because the synthesis of such nanostructures involves interactions between a large number of short oligonucleotides, the yield of complete structures is highly sensitive to stoichiometry (the relative ratios of strands). The synthesis of relatively complex structures was thus thought to require multiple reaction steps and purifications, with the ultimate complexity of DNA nanostructures limited by necessarily low yields. Recently, the controlled folding of a long single DNA strand into an octahedron was reported[14], an approach that may be thought of as 'single-stranded DNA origami'. The success of this work suggested that the folding of long strands could, in principle, proceed without many misfoldings and avoid the problems of stoichiometry and purification associated with methods that use many short DNA strands.

I now present a versatile and simple 'one-pot' method for using numerous short single strands of DNA to direct the folding of a long, single strand of DNA into desired shapes that are roughly 100 nm in diameter and have a spatial resolution of about 6 nm. I demonstrate the generality of this method, which I term 'scaffolded DNA origami', by assembling six different shapes, such as squares, triangles and five-pointed stars. I show that the method not only provides access to structures that approximate the outline of any desired shape, but also enables the creation of structures with arbitrarily shaped holes or surface patterns composed of more than 200 individual pixels. The patterns on the 100-nm-sized DNA shapes thus have a complexity that is tenfold higher than that of any previously self-assembled arbitrary pattern and comparable to that achieved using AFM and STM surface manipulation[4].

Design of scaffolded DNA origami

The design of a DNA origami is performed in five steps, the first two by hand and the last three aided by computer (details in Supplementary Note S1). The first step is to build a geometric model of a DNA structure that will approximate the desired shape. Figure 1a shows an example shape (outlined in red) that is 33 nm wide and 35 nm tall. The shape is filled from top to bottom by an even number of parallel double helices, idealized as cylinders. The helices are cut to fit the shape in sequential pairs and are constrained to be an integer number of turns in length. To hold the helices together, a periodic array of crossovers (indicated in Fig. 1a as small blue crosses) is incorporated; these crossovers designate positions at which strands running along one helix switch to an adjacent helix and continue there. The resulting model approximates the shape within one turn (3.6 nm) in the x-direction and roughly two helical widths (4 nm) in the

[1]Departments of Computer Science and Computation & Neural Systems, California Institute of Technology, Pasadena, California 91125, USA.

y-direction. As noticed before in DNA lattices[15], parallel helices in such structures are not close-packed, perhaps owing to electrostatic repulsion. Thus the exact *y*-resolution depends on the gap between helices. The gap, in turn, appears to depend on the spacing of crossovers. In Fig. 1a crossovers occur every 1.5 turns along alternating sides of a helix, but any odd number of half-turns may be used. In this study, data are consistent with an inter-helix gap of 1 nm for 1.5-turn spacing and 1.5 nm for 2.5-turn spacing, yielding a *y*-resolution of 6 or 7 nm, respectively.

Conceptually, the second step (illustrated in Fig. 1b) proceeds by folding a single long scaffold strand (900 nucleotides (nt) in Fig. 1b) back and forth in a raster fill pattern so that it comprises one of the two strands in every helix; progression of the scaffold from one helix to another creates an additional set of crossovers, the 'scaffold crossovers' (indicated by small red crosses in Fig. 1b). The fundamental constraint on a folding path is that the scaffold can form a crossover only at those locations where the DNA twist places it at a tangent point between helices. Thus for the scaffold to raster progressively from one helix to another and onto a third, the distance between successive scaffold crossovers must be an odd number of half turns. Conversely, where the raster reverses direction vertically and returns to a previously visited helix, the distance between scaffold crossovers must be an even number of half-turns. Note that the folding path shown in Fig. 1b is compatible with a circular scaffold and leaves a 'seam' (a contour which the path does not cross).

Once the geometric model and a folding path are designed, they are represented as lists of DNA lengths and offsets in units of half-turns. These lists, along with the DNA sequence of the actual scaffold to be used, are input to a computer program. Rather than assuming 10.5 base pairs (bp) per turn (which corresponds to standard B-DNA twist), the program uses an integer number of bases between periodic crossovers (for example, 16 bp for 1.5 turns). It then performs the third step, the design of a set of 'staple strands' (the coloured DNA strands in Fig. 1c) that provide Watson–Crick complements for the

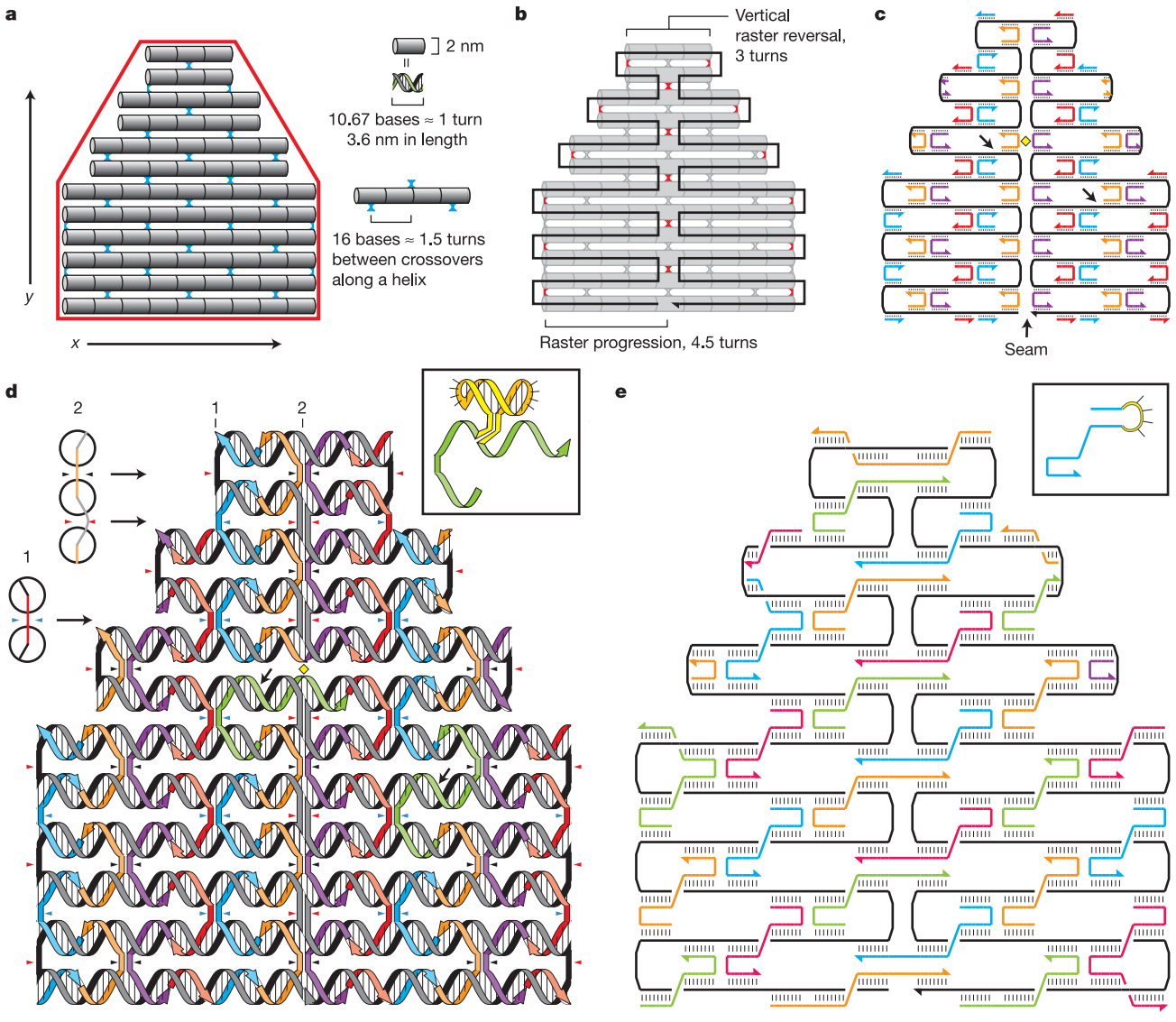

Figure 1 | Design of DNA origami. **a**, A shape (red) approximated by parallel double helices joined by periodic crossovers (blue). **b**, A scaffold (black) runs through every helix and forms more crossovers (red). **c**, As first designed, most staples bind two helices and are 16-mers. **d**, Similar to **c** with strands drawn as helices. Red triangles point to scaffold crossovers, black triangles to periodic crossovers with minor grooves on the top face of the shape, blue triangles to periodic crossovers with minor grooves on bottom. Cross-sections of crossovers (1, 2, viewed from left) indicate backbone positions with coloured lines, and major/minor grooves by large/small angles between them. Arrows in **c** point to nicks sealed to create green strands in **d**. Yellow diamonds in **c** and **d** indicate a position at which staples may be cut and resealed to bridge the seam. **e**, A finished design after merges and rearrangements along the seam. Most staples are 32-mers spanning three helices. Insets show a dumbbell hairpin (**d**) and a 4-T loop (**e**), modifications used in Fig. 3.

scaffold and create the periodic crossovers. Staples reverse direction at these crossovers; thus crossovers are antiparallel, a stable configuration well characterized in DNA nanostructures[16]. Note that the crossovers in Fig. 1c are drawn somewhat misleadingly, in that single-stranded regions appear to span the inter-helix gap even though the design leaves no bases unpaired. In the assembled structures, helices are likely to bend gently to meet at crossovers so that only a single phosphate from each backbone occurs in the gap (as ref. 16 suggests for similar structures). Such small-angle bending is not expected to greatly affect the width of DNA origami (see also Supplementary Note S2).

The minimization and balancing of twist strain between crossovers is complicated by the non-integer number of base pairs per half-turn (5.25 in standard B-DNA) and the asymmetric nature of the helix (it has major and minor grooves). Therefore, to balance the strain[15] caused by representing 1.5 turns with 16 bp, periodic crossovers are arranged with a glide symmetry, namely that the minor groove faces alternating directions in alternating columns of periodic crossovers (see Fig. 1d, especially cross-sections 1 and 2). Scaffold crossovers are not balanced in this way. Thus in the fourth step, the twist of scaffold crossovers is calculated and their position is changed (typically by a single bp) to minimize strain; staple sequences are recomputed accordingly. Along seams and some edges the minor groove angle (150°) places scaffold crossovers in tension with adjacent periodic crossovers (Fig. 1d, cross-section 2); such situations are left unchanged.

Wherever two staples meet there is a nick in the backbone. Nicks occur on the top and bottom faces of the helices, as depicted in Fig. 1d. In the final step, to give the staples larger binding domains with the scaffold (in order to achieve higher binding specificity and higher binding energy which results in higher melting temperatures), pairs of adjacent staples are merged across nicks to yield fewer, longer, staples (Fig. 1e). To strengthen a seam, an additional pattern of breaks and merges may be imposed to yield staples that cross the seam; a seam spanned by staples is termed 'bridged'. The pattern of merges is not unique; different choices yield different final patterns of nicks and staples. All merge patterns create the same shape but, as shown later, the merge pattern dictates the type of grid underlying any pixel pattern later applied to the shape.

Folding M13mp18 genomic DNA into shapes

To test the method, circular genomic DNA from the virus M13mp18 was chosen as the scaffold. Its naturally single-stranded 7,249-nt sequence was examined for secondary structure, and a hairpin with a 20-bp stem was found. Whether staples could bind at this hairpin was unknown, so a 73-nt region containing it was avoided. When a linear scaffold was required, M13mp18 was cut (in the 73-nt region) by digestion with *Bsr*BI restriction enzyme. While 7,176 nt remained available for folding, most designs did not fold all 7,176 nt; short (≤25 nt) 'remainder strands' were added to complement unused sequence. In general, a 100-fold excess of 200–250 staple and remainder strands were mixed with scaffold and annealed from

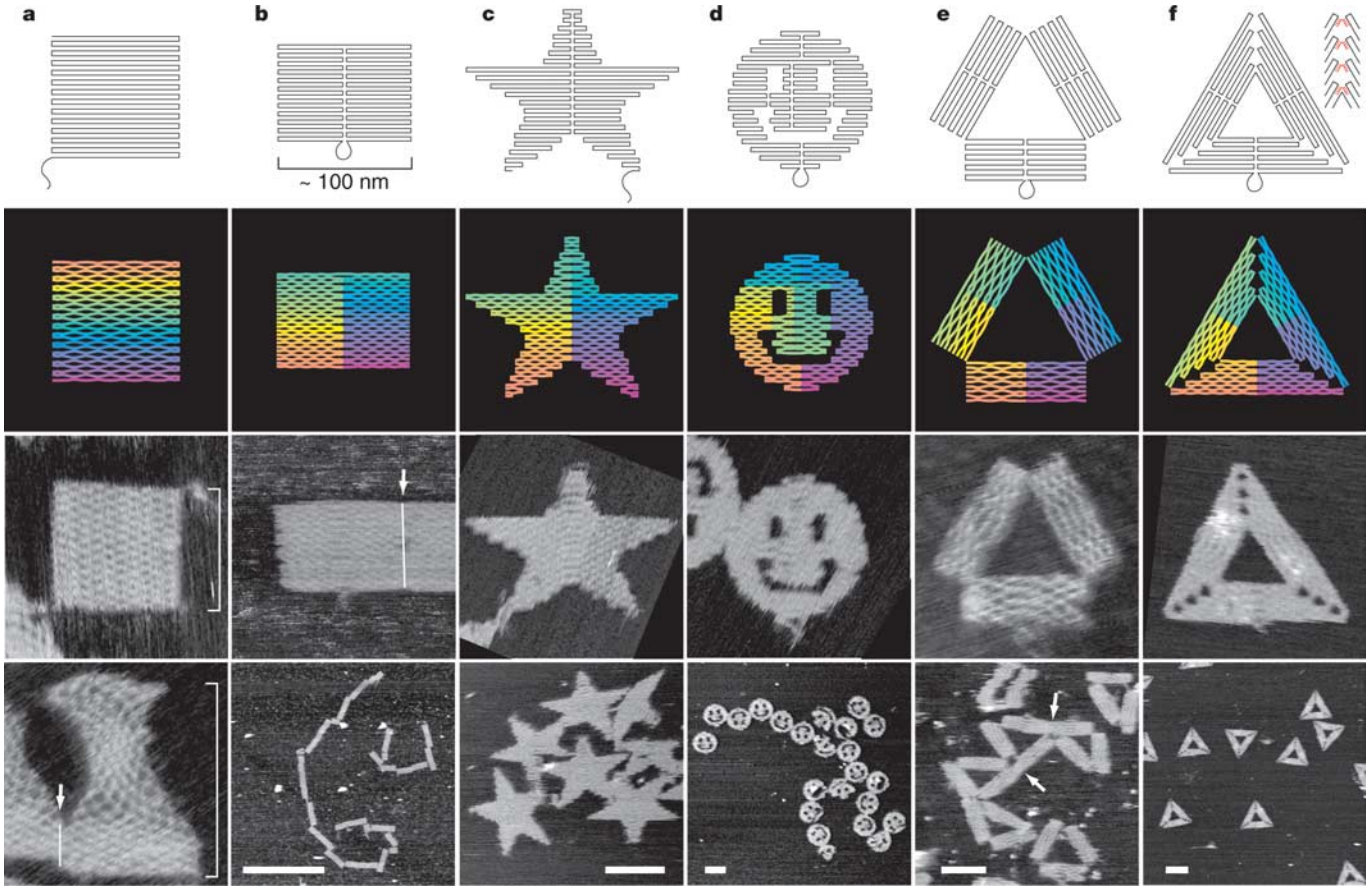

Figure 2 | DNA origami shapes. Top row, folding paths. **a**, square; **b**, rectangle; **c**, star; **d**, disk with three holes; **e**, triangle with rectangular domains; **f**, sharp triangle with trapezoidal domains and bridges between them (red lines in inset). Dangling curves and loops represent unfolded sequence. Second row from top, diagrams showing the bend of helices at crossovers (where helices touch) and away from crossovers (where helices bend apart). Colour indicates the base-pair index along the folding path; red is the 1st base, purple the 7,000th. Bottom two rows, AFM images. White lines and arrows indicate blunt-end stacking. White brackets in **a** mark the height of an unstretched square and that of a square stretched vertically (by a factor >1.5) into an hourglass. White features in **f** are hairpins; the triangle is labelled as in Fig. 3k but lies face down. All images and panels without scale bars are the same size, 165 nm × 165 nm. Scale bars for lower AFM images: **b**, 1 μm; **c**–**f**, 100 nm.

95 °C to 20 °C in <2 h. When samples were deposited on mica, only folded DNA structures stuck to the surface while excess staples remained in solution; AFM imaging thus proceeded under buffer without prior purification. Six different folds were explored; Fig. 2 gives their folding paths and their predicted and experimentally observed DNA structures. (Models and staple sequences are given in Supplementary Note S3, final designs appear in Supplementary Note S12. Experimental methods are given in Supplementary Note S4, results described here but not shown are in Supplementary Note S5.) Of the products imaged by AFM, a particular structure was considered qualitatively 'well-formed' if it had no defect (hole or indentation in the expected outline) greater than 15 nm in diameter. For each fold the fraction of well-formed structures, as a percentage of all distinguishable structures in one or more AFM fields, was calculated as a rough estimate of yield. I note that while some structures classified as well-formed had 15-nm defects, most had no defects greater than 10 nm in diameter.

First, a simple 26-helix square was designed (Fig. 2a). The square had no vertical reversals in raster direction, required a linear scaffold, and used 2.5-turn crossover spacing. Most staples were 26-mers that bound each of two adjacent helices as in Fig. 1c, but via 13 bases rather than 8. The design was made assuming a 1.5-nm inter-helix gap; an aspect ratio of 1.05 (93.9 nm × 89.5 nm) was expected. By AFM, 13% of structures were well-formed squares (out of $S = 45$ observed structures) with aspect ratios from 1.00 to 1.07 and bore the expected pattern of crossovers (Fig. 2a, upper AFM image). Of the remaining structures, ~25% were rectangular fragments, and ~25% had an hourglass shape that showed a continuous deformation of the crossover lattice (Fig. 2a, lower AFM image). Sequential imaging documented the stretching of a square into an hourglass, suggesting that hourglasses were originally squares that stretched upon deposition or interaction with the AFM tip. No subsequent designs exhibited stretching. Other designs had either a tighter 1.5-turn spacing with 32-mer staples spanning three helical domains (Fig. 2b–d, f) or smaller domains that appeared to slide rather than stretch (Fig. 2e).

To test the formation of a bridged seam, a rectangle was designed (Fig. 2b) according to the scheme outlined in Fig. 1e using 1.5-turn crossover spacing, 32-mer staples and a circular scaffold. As seen in Fig. 2b, the central seam and associated pattern of crossovers was easily visualized (upper AFM image). Rectangles stacked along their vertical edges, often forming chains up to 5 μm long (lower AFM image). The yield of well-formed rectangles was high (90%, $S = 40$), and so rectangles were used to answer basic questions concerning inter-helix gaps, base-stacking, defects and stoichiometry. AFM drift

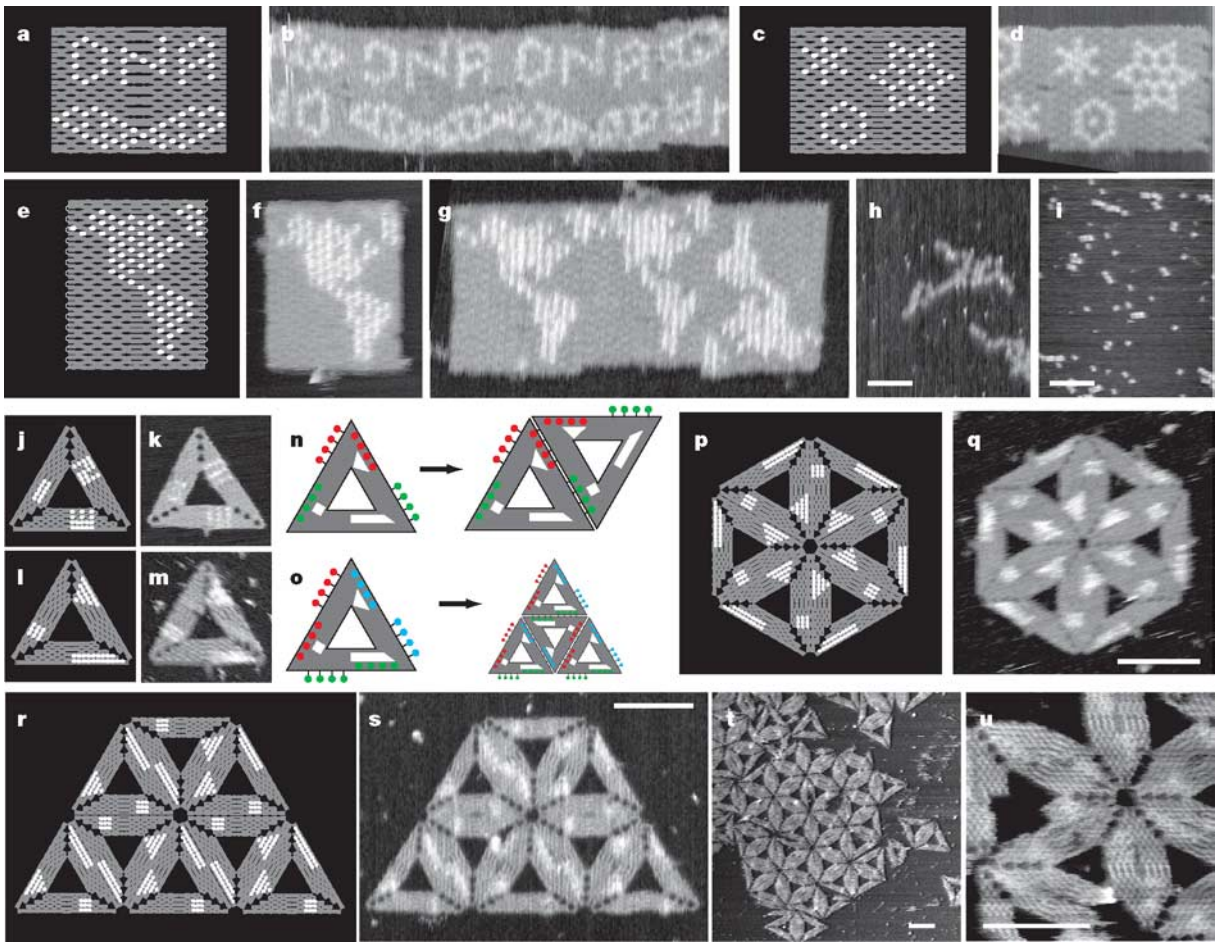

Figure 3 | **Patterning and combining DNA origami. a**, Model for a pattern representing DNA, rendered using hairpins on a rectangle (Fig. 2b). **b**, AFM image. One pixelated DNA turn (~100 nm) is 30× the size of an actual DNA turn (~3.6 nm) and the helix appears continuous when rectangles stack appropriately. Letters are 30 nm high, only 6× larger than those written using STM in ref. 3; 50 billion copies rather than 1 were formed. **c**, **d**, Model and AFM image, respectively, for a hexagonal pattern that highlights the nearly hexagonal pixel lattice used in **a**–**i**. **e**–**i**, Map of the western hemisphere, scale 1:2 × 10^{14}, on a rectangle of different aspect ratio. Normally such rectangles aggregate (**h**) but 4-T loops or tails on edges (white lines in **e**) greatly decrease stacking (**i**). **j**–**m**, Two labellings of the sharp triangle show that each edge may be distinguished. In **j**–**u**, pixels fall on a rectilinear lattice. **n**–**u**, Combination of sharp triangles into hexagons (**n**, **p**, **q**) or lattices (**o**, **r**–**u**). Diagrams (**n**, **o**) show positions at which staples are extended (coloured protrusions) to match complementary single-stranded regions of the scaffold (coloured holes). Models (**p**, **r**) permit comparison with data (**q**, **s**). The largest lattice observed comprises only 30 triangles (**t**). **u** shows close association of triangles (and some breakage). **d** and **f** were stretched and sheared to correct for AFM drift. Scale bars: **h**, **i**, 1 μm; **q**, **s**–**u**, 100 nm.

often distorts aspect ratios so that inter-helix gaps cannot be inferred from the aspect ratio of a single rectangle. A range of aspect ratios implied a gap size from 0.9 to 1.2 nm; later designs assume 1 nm. Whatever the exact value, it is consistent: aspect ratios were invariant along stacked chains with dozens of rectangles. Such stacking was almost completely abolished by omitting staples along vertical edges. On the other hand, stacking across the seam of an unbridged rectangle (as in Fig. 1c) kept 65% of structures ($S = 40$) well-formed; the rest showed some degree of dislocation at the seam. Other defects, such as the intentional omission of single staples, could be visualized as 5–10-nm holes. However, sharp tips and high tapping amplitudes were required; repeated scanning created holes difficult to distinguish from holes due to missing strands. This effect also increased uncertainty when stoichiometry was varied. When staple excesses of approximately 100:1 and 9:1 were used, the frequencies of 5–10-nm holes (a few per rectangle) were indistinguishable. At 2:1, rectangles were similar; perhaps a greater fraction were malformed. At 1.5:1, rectangles formed but had holes up to ~10% of their area in size. At a 1:1 ratio, <1% of structures were rectangular.

To demonstrate the creation of arbitrary shapes, a five-pointed star was designed with 1.5-turn spacing, 32-mer staples and a linear rather than circular scaffold (Fig. 2c). Designed assuming a 1.5-nm inter-helix gap (the work was carried out before the gap for 1.5-turn spacing was measured), the stars are somewhat squat (Fig. 2c, upper AFM image). Still, the stars show that the width of a shape may be approximated to within one DNA turn. Many of the structures observed were star fragments (Fig. 2c, lower AFM image), and only 11% ($S = 70$) were well-formed. The low yield of stars (and squares, see above) may be due to strand breakage occurring during *Bsr*BI digestion or subsequent steps to remove the enzyme; when untreated circular scaffold was folded into stars, 63% ($S = 43$) were well-formed. To show that DNA origami need not be topological disks, and that scaffolds can be routed arbitrarily through shapes, a three-hole disk was designed (Fig. 2d). Although the shape approximated is symmetric, the folding path is highly asymmetric and has five distinct seams. Unlike the rectangles, which rarely break or fold, three-hole disks exhibit several characteristic deformations (Fig. 2d, lower AFM image); still, 70% ($S = 90$) were well-formed.

DNA origami is not limited to the approximation of shapes by raster fill: some shapes can be created more exactly by combining distinct raster fill domains in non-parallel arrangements. Figure 2e shows a triangle built from three separate, 2.5-turn spacing rectangular domains; only single covalent bonds along the scaffold hold the domains together. But the desired equiangular triangles (upper AFM image) were rarely observed (<1%, $S = 199$). As seen in the lower AFM image, stacking caused rectangular domains of separate triangles to bind; this effect and the flexibility of the single-bond joints at the vertices may account for the ease with which these triangles deform. To solve these problems, 'sharp triangles', built from trapezoidal domains with 1.5-turn spacing, were designed (Fig. 2f). The slanted edges of the trapezoids meet at the triangle vertices and allow the addition of bridging staples along these interfaces. Sharp triangles remained separated and equiangular (Fig. 2f, lower AFM image); 88% were well-formed ($S = 78$). Even when bridging staples at the vertices were not used, a large number of sharp triangles were well-formed (55%, $S = 22$). These 'weakened' sharp triangles provided the most stringent test of the estimated inter-helix gap, because too high or low an estimate would have caused gaps or overlaps between trapezoids. Gaps of 10 nm occasionally appeared but overlaps were never observed, suggesting that 1 nm may be a slight underestimate of the inter-helix gap.

Patterning and combining DNA origami

In addition to binding the DNA scaffold and holding it in shape, staple strands provide a means for decorating shapes with arbitrary patterns of binary pixels. Given a shape, the original set of staples is taken to represent binary '0's; a new set of labelled staples, one for each original staple, is used to represent binary '1's. Patterns are created by mixing appropriate subsets of these strands. In this way, any desired pattern can be made.

In principle, a variety of DNA modifications—for example, biotin or fluorophores—could serve as labels. Here, 'dumbbell hairpins' (Fig. 1d inset, Supplementary Note S6), designed to avoid dimerization at high concentration, were added to the middle of 32-mer staples at the position of merges made during design. Depending on the merge pattern, the resulting pixel pattern was either rectilinear, with adjacent columns of hairpins on alternate faces of the shape, or staggered and nearly hexagonally packed, with all hairpins on the same face. In AFM images labelled staples give greater height contrast (3 nm above the mica) than unlabelled staples (~1.5 nm), which results in a pattern of light '1' and dark '0' pixels. Several patterns (Fig. 3), each with ~200 pixels, illustrate the generality of this technique.

Yields of patterned origami were similar to those of unpatterned origami; for the pattern in Fig. 3a, 91% ($S = 85$) of rectangles were well-formed. Because rectilinear patterns imaged poorly, only staggered patterns were examined quantitatively. Distances measured between pairs of '1' pixels in alternating columns (two pixel widths: 11.5 ± 0.9 nm, mean ± s.d., $n = 26$) and adjacent rows (one pixel height: 6.6 ± 0.5 nm, $n = 24$) are consistent with the theoretically expected pixel size of 5.4 nm × 6 nm. Most defects take the form of 'missing pixels'; that is, pixels that should image as '1's but image as '0's instead. 94% of '1' pixels (of 1,080 observed) were visualized. Whether missing pixels represent real defects or artefacts of imaging is unknown; sequential AFM images occasionally showed '1' pixels that later converted irreversibly to '0' pixels, suggesting tip-induced damage. Stoichiometric errors, synthetic errors, or unwanted secondary structure are not implicated for any particular strand, as the position of missing pixels appeared random (Fig. 3b, f and g).

Stacking of shapes along blunt-ended helices provides an uncontrolled mechanism for the creation of larger structures (Fig. 3b). Instead of removing staples on the edge of a rectangle to avoid stacking (as described previously), 4-T hairpin loops (four thymines in a row, Fig. 1e, inset) or 4-T tails can be added to edge staples (Fig. 3e, f); stacked chains of 3–5 rectangles still formed (Fig. 3g), but 30% of rectangles ($S = 319$) occurred as monomers (Fig. 3i). Without hairpins, all rectangles occurred in aggregates (Fig. 3h).

Controlled combination of shapes was achieved by designing 'extended staples' that connected shapes along their edges. To create a binding interaction between two particular edges, extended staples were designed by merging and breaking normal staples along these edges (Supplementary Note S7). Starting with sharp triangles, this approach was used to create finite (hexagons; Fig. 3n, p, q) as well as periodic structures (triangular lattice; Fig. 3o, r–u). I note that the successful combination of shapes (unlike the successful formation of individual shapes) is in principle very sensitive to the concentrations of extended staples (which should ideally be equal to that of the scaffold). Poor stoichiometry may play a role in the poor yield of hexagons (<2%, $S = 70$) and lattices (not measured).

Discussion

The scaffolded self-assembly of DNA strands has been used to create linear structures[17,18] and proposed as a method for creating arbitrary patterns[18,19]. But the widespread use of scaffolded self-assembly, and in particular the use of long DNA scaffolds in combination with hundreds of short strands, has been inhibited by several misconceptions: it was assumed that (1) sequences must be optimized[20] to avoid secondary structure or undesired binding interactions, (2) strands must be highly purified, and (3) strand concentrations must be precisely equimolar. These three criteria are important for the formation of many DNA nanostructures and yet all three are ignored in the present method. For example, M13mp18 is essentially a natural sequence that has a predicted secondary structure which is more stable (lower in energy) than similar random sequences

(Supplementary Note S8). Further, stocks of staples each contained a few per cent truncation products, stock concentrations were measured with at least 10% error, and staples were used successfully at stoichiometries that varied over an order of magnitude.

I suggest that several factors contribute to the success of scaffolded DNA origami (even though the method ignores the normal, careful practices of DNA nanotechnology). These are (1) strand invasion, (2) an excess of staples, (3) cooperative effects and (4) design that intentionally does not rely on binding between staples. Briefly (details are given in Supplementary Note S9), strand invasion may allow correct binding of excess full-length staples to displace unwanted secondary structure, incorrect staples, or grossly truncated staples. Further, each correct addition of a staple organizes the scaffold for subsequent binding of adjacent staples and precludes a large set of undesired secondary structures. Last, because staples are not designed to bind one another, their relative concentrations do not matter.

The method presented here is easy to implement, high yield and relatively inexpensive. Three months of effort went into the design program. In addition, each structure required about one week to design and one week to synthesize (commercially); the mixing and annealing of strands required a few hours. The greatest experimental difficulty was acquiring high-resolution AFM images, typically taking two days per structure. For rigid designs using circular scaffolds (rectangles with patterns, three-hole disks, and sharp triangles), yields of qualitatively well-formed structures were at least 70%. A better understanding of folding will depend on less-destructive imaging and quantification of small ($<$15 nm) defects. A possible objection to the routine use of the method is the potential cost of staples; unlike the scaffold, staples cannot be cloned. However, unpurified strands are inexpensive so that the scaffold constitutes 80% of the cost, even when using a 100-fold excess of staples (Supplementary Note S10).

I believe that scaffolded DNA origami can be adapted to create more complex or larger structures. For example, the design of three-dimensional structures should be accessible using a straightforward adaptation of the raster fill method given here. If non-repetitive scaffolds of megabase length can be prepared, micrometre-size origami with 20,000 features may be possible. However, the requirement for unique sequence information means that the method cannot be scaled up arbitrarily; whenever structures above a critical size or level of complexity are desired, it will therefore be necessary to combine scaffolded DNA origami with hierarchical self-assembly[10,11], algorithmic self-assembly[22], or top-down fabrication techniques.

An obvious application of patterned DNA origami would be the creation of a 'nanobreadboard', to which diverse components could be added. The attachment of proteins[23], for example, might allow novel biological experiments aimed at modelling complex protein assemblies and examining the effects of spatial organization, whereas molecular electronic or plasmonic circuits might be created by attaching nanowires, carbon nanotubes or gold nanoparticles[24]. These ideas suggest that scaffolded DNA origami could find use in fields as diverse as molecular biology and device physics.

Received 7 September 2005; accepted 12 January 2006.

1. Feynman, R. P. There's plenty of room at the bottom. *Engineering and Science* 23(5), 22–36 (Caltech, February, 1960).
2. Junno, T., Deppert, K., Montelius, L. & Samuelson, L. Controlled manipulation of nanoparticles with an atomic force microscope. *Appl. Phys. Lett.* **66,** 3627–3629 (1995).
3. Eigler, D. M. & Schweizer, E. K. Positioning single atoms with a scanning tunnelling microscope. *Nature* **344,** 524–526 (1990).
4. Heinrich, A. J., Lutz, C. P., Gupta, J. A. & Eigler, D. M. Molecular cascades. *Science* **298,** 1381–1387 (2002).
5. Whitesides, G. M., Mathias, J. P. & Seto, C. T. Molecular self-assembly and nanochemistry: a chemical strategy for the synthesis of nanostructures. *Science* **254,** 1312–1319 (1991).
6. Yokoyama, T., Yokoyama, S., Kamikado, T., Okuno, Y. & Mashiko, S. Self-assembly on a surface of supramolecular aggregates with controlled size and shape. *Nature* **413,** 619–621 (2001).
7. Mao, C. B. *et al.* Virus-based toolkit for the directed synthesis of magnetic and semiconducting nanowires. *Science* **303,** 213–217 (2004).
8. Seeman, N. C. Nucleic-acid junctions and lattices. *J. Theor. Biol.* **99,** 237–247 (1982).
9. Seeman, N. C. & Lukeman, P. S. Nucleic acid nanostructures: bottom-up control of geometry on the nanoscale. *Rep. Prog. Phys.* **68,** 237–270 (2005).
10. Chworos, A. *et al.* Building programmable jigsaw puzzles with RNA. *Science* **306,** 2068–2072 (2004).
11. Park, S. H. *et al.* Finite-size, fully-addressable DNA tile lattices formed by hierarchical assembly procedures. *Angew. Chem.* **118,** 749–753 (2006).
12. Chen, J. & Seeman, N. C. The synthesis from DNA of a molecule with the connectivity of a cube. *Nature* **350,** 631–633 (1991).
13. Zhang, Y. & Seeman, N. C. The construction of a DNA truncated octahedron. *J. Am. Chem. Soc.* **116,** 1661–1669 (1994).
14. Shih, W. M., Quispe, J. D. & Joyce, G. F. A 1.7-kilobase single-stranded DNA that folds into a nanoscale octahedron. *Nature* **427,** 618–621 (2004).
15. Rothemund, P. W. K. *et al.* Design and characterization of programmable DNA nanotubes. *J. Am. Chem. Soc.* **26,** 16344–16353 (2004).
16. Fu, T.-J. & Seeman, N. C. DNA double-crossover molecules. *Biochemistry* **32,** 3211–3220 (1993).
17. LaBean, T. H., Winfree, E. & Reif, J. H. in *DNA Based Computers V* (eds Winfree, E. & Gifford, D. K.) 123–140 (Vol. 54 of DIMACS, AMS Press, Providence, Rhode Island, 1999).
18. Yan, H., LaBean, T. H., Feng, L. & Reif, J. H. Directed nucleation assembly of DNA tile complexes for barcode-patterned lattices. *Proc. Natl Acad. Sci. USA* **100,** 8103–8108 (2003).
19. Reif, J. H. in *Proc. 29th Int. Colloquium on Automata, Languages, and Programming (ICALP)* (eds Widmayer, P., Ruiz, F. T., Bueno, R. M., Hennessy, M., Eidenbenz, S. & Conejo, R.) 1–21 (Vol. 2380 of Lecture Notes in Computer Science, Springer, New York, 2002).
20. Seeman, N. C. *De novo* design of sequences for nucleic acid structural engineering. *J. Biomol. Struct. Dyn.* **8,** 573–581 (1990).
21. Winfree, E. in *DNA Based Computers* (eds Lipton, R. J. & Baum, E. B.) 199–221 (Vol. 27 of DIMACS, AMS Press, Providence, Rhode Island, 1996).
22. Rothemund, P. W. K., Papadakis, N. & Winfree, E. Algorithmic self-assembly of DNA Sierpinski triangles. *PLoS Biol.* **2,** e424 (2004).
23. Yan, H., Park, S. H., Finkelstein, G., Reif, J. H. & LaBean, T. H. DNA-templated self-assembly of protein arrays and highly conductive nanowires. *Science* **301,** 1882–1884 (2003).
24. Le, J. D. *et al.* DNA-templated self-assembly of metallic nanocomponent arrays on a surface. *Nano Lett.* **4,** 2343–2347 (2004).

Supplementary Information is linked to the online version of the paper at www.nature.com/nature.

Acknowledgements I thank E. Winfree for discussions and providing a stimulating laboratory environment; B. Yurke for the term 'nanobreadboard'; N. Papadakis, L. Adleman, J. Goto, R. Barish, R. Schulman, R. Hariadi, M. Cook and M. Diehl for discussions; B. Shaw for a gift of AFM tips; A. Schmidt for coordinating DNA synthesis; and K. Yong, J. Crouch and L. Hein for administrative support. This work was supported by National Science Foundation Career and Nano grants to E. Winfree as well as fellowships from the Beckman Foundation and Caltech Center for the Physics of Information.

Author Information Reprints and permissions information is available at npg.nature.com/reprintsandpermissions. The author declares competing financial interests: details accompany the paper on www.nature.com/nature. Correspondence and requests for materials should be addressed to P.W.K.R. (pwkr@dna.caltech.edu).